

## The Influence of Bimodal Heterogeneity on Viscous Fingering of a Miscible Interface in Porous Media

Mozhdeh Sajjadi\*

Institute of Petroleum Engineering, College of Engineering, University of Tehran, Tehran, Iran. E-mail: Sajjadi.mozhdeh@ut.ac.ir

ARTICLE INFO	ABSTRACT
<p><b>Article History:</b> Received: 29 August 2021 Revised: 30 September 2021 Accepted: 01 October 2021</p> <p><b>Article type:</b> Research</p> <p><b>Keywords:</b> Bimodal Porosity, Channeling, Heterogeneity, Hydrodynamic Instability, Layered Medium, Miscible Displacement, Viscous Fingering</p>	<p>The flow regimes and the dynamics of the front in miscible displacements are controlled by the interactions between the mechanisms of instability involved in such processes. The instabilities may be driven by the unfavorable relative characteristics of the fluids (like unfavorable gravity or mobility ratios) or by the heterogeneity of the medium, providing favorable paths for the more mobile fluid. This work investigates the effect of porous medium heterogeneity with two scales of permeability variations on the frontal instability and fluid mixing. The base mode of permeability variations has a smaller wavelength and higher frequency, while the imposed mode has a larger wavelength. The effect of such a bimodal heterogeneity on the growth of mixing zone length (MZL) has been studied and the development of the previously recognized flow regimes in layered porous media have been examined. The combination of a short wave which induces faster growth of instabilities at initial stages of the flow, and a relatively longer wavelength heterogeneity with elongated channeling period, distorts the consecutive appearance of the flow regimes observed in single wavelength heterogeneity profiles of previous studies. Compared to the unimodal medium comprising the base wave, in the bimodal cases with large contrast between the wavelengths of the two periodic profiles the dominance of each wavelength at a different time scale predictably enhances the growth of fingers in the early and late stages. Interestingly and less intuitively, even in cases with close wave numbers between the combined modes (e.g. 15 layers combined with 11 layers) faster growth of the mixing zone length is observed. In such cases, the coherence of equal layers in a unimodal layered medium is disturbed by the second wave number, which results in fading of the lateral diffusion regime. However, bimodal heterogeneity may attenuate the instability compared to the unimodal system with the imposed wave's frequency.</p>

### Introduction

Miscible displacement and fluid mixing in porous media are faced in various applications like contaminant transport [1], chromatography in packed beds [2], miscible oil displacement [3], CO<sub>2</sub> flooding and storage [4], and polymer slug injection projects [5]. The interface between the fluids is often unstable due to the unfavorable ratio between the fluid properties (e.g., viscosity and density) or the heterogeneity in the porous medium. The instability shows itself in the form of advancing fingers of displacing fluid, bypassing the in-situ fluid. When

\* Corresponding Author: M.Sajjadi (E-mail address: Sajjadi.mozhdeh@ut.ac.ir)



triggered by the viscosity mismatch between the fluids, it is referred to as viscous fingering. The interaction between viscous instability and the heterogeneity of the medium in miscible displacements is interesting from many aspects. Despite the vast number of studies on experimental, analytical, and numerical investigation of the effect of heterogeneity on viscous fingering [4, 6, 7, 8], the exact mechanism is not fully understood, and one cannot predict the rate of mixing, breakthrough time, or other important measurable parameters for complex heterogeneity models. In displacement processes, the heterogeneity of the porous medium affects viscous fingering at different scales and changes the mixing mechanisms during different flow regimes. One of the simple forms of heterogeneity is periodically varying permeability across the flow domain, forming a layered system, first defined by De Wit and Homsy [6]. The studies on layered porous media with periodic heterogeneity across the domain have revealed four flow regimes, including an initial diffusive flow, the channeling regime, transverse diffusion, and finally, the viscous fingering regime [7]. The flow regimes and the dynamics of the miscible displacements are customarily characterized using mixing zone length (MZL) defined as the length of the region with a transverse average concentration between 0.01 and 0.99. Other definitions have been proposed for MZL (e.g., using the concentration variance about the initial condition [8]), which are believed to capture some flow behavior more accurately, but in this work, we use the old fashion definition to be comparable to our previous studies. Regardless of the definition, fast growth of MZL is interpreted as the rapid growth of instabilities on the front zone, and slower growth of MZL is usually attributed to a diffusive flow behavior. The study of MZL growth in layered media has shown that the heterogeneity characteristics of the rock (i.e., heterogeneity length scale and permeability variance), along with the displacement parameters (i.e. the flow rate, the diffusion coefficient, and the mobility ratio of the components) affect the development of the flow regimes and the time scale of the events [7].

Despite the comprehensive study conducted on the periodic variation of permeability with a single wavelength, the effect of a second wavelength (like what is observed in bimodal permeability [4, 9]) has not received much attention. Although bimodal heterogeneity can be correlated to fractured media, in which the variation of permeability inside the matrix is widely different from the fissure network, there are other formations with similar order of permeability variation at different scales [10]. Bimodal heterogeneity is recognized for different reservoir rocks. Specifically, in carbonate rocks the micro-pores between clay crystals form preferred channels for flow in micro scale (Fig. 1). A bundle of these micro-channels forms a flow path between the rock grains in a larger scale. The variation of density of grains in different regions changes the permeability over longer distances. Thus, the heterogeneity can be characterized in different scales. If the heterogeneity correlation length is small at one scale its effect can be discounted or modeled through a modified diffusion rate. In their simulations, Sajjadi and Azaiez [7] showed that in periodically layered media, the dimensionless group  $\frac{w/L}{Pe}$  ( $w$ : width of the layers,  $L$ : length of the medium, and  $Pe$ : Peclet number) defines the flow characteristics and the time scale and length scale of the flow regimes. According to their simulation results, for  $\frac{w/L}{Pe} \leq 10$  the fingering patterns in periodically layered media were identical to those in homogeneous media. However, for channels of larger widths ( $\frac{w/L}{Pe} > 10$ ) the heterogeneity of the medium affected the displacement front's stability and the mixing process.

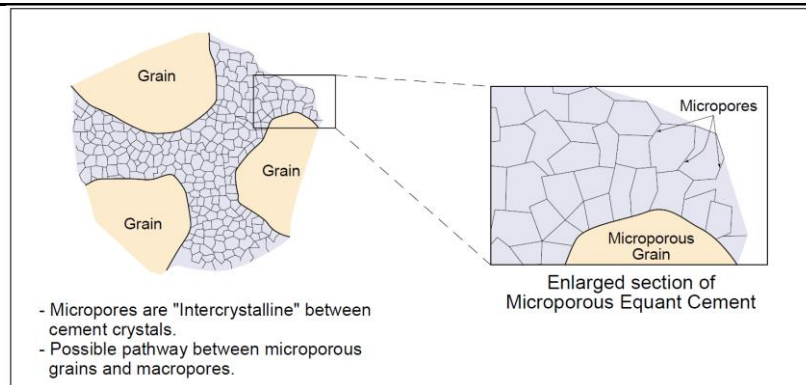


**Fig. 1.** Bimodal structure of a carbonate rock sample from the Arab formation [9]

From a mathematical point of view, bimodal heterogeneity may be defined based on the frequency or the length scale of permeability variations. Accordingly, when two peaks are observed in the histogram of permeability [11] or when the medium has two length scales of permeability variation [10], bimodal heterogeneity may be perceived. Due to the determinative role of heterogeneity length scale on the flow behavior, in this work the second definition, namely two wavelengths of permeability variations has been employed. In 1995, Rubin [10] developed a probabilistic description of permeability variation using a spatially random function with two length scales representing the two modes of heterogeneity. The analytical work of Rubin focused on the probabilistic characteristics of the domain, so the results could be generalized to any random permeability distribution. But the definition of random permeability profile for numerical simulations makes the observed phenomena to be case-specific. So the measurable properties such as the growth rate of mixing zone length may be different for two different random permeability realizations with the same length scales. To overcome this limitation, in the current study, the bimodal heterogeneity is defined by considering the variations only in a transverse direction and combining a short wave periodic permeability forming the base wave with a relatively longer wavelength variation (here called the imposed wave). Practically the base mode of heterogeneity can be deemed as the micropores between the crystalline or at a larger scale as the heterogeneities within a geological layer. Likewise, the imposed wave can resemble the grouped crystalline between the grains or the geological layers with different permeabilities. This definition is a simplified scheme compared to the probability density functions capable of realization of two-dimensional random permeability distributions. Yet, as will be discussed in the results section, the flow behavior in the presence of the different length scales of permeability variations matches the results of previous studies qualitatively. In addition to capturing the essential behavior, such a simplified definition allows for in depth analysis of the flow regimes and each length scale's contribution to flow instability, which cannot be obtained in more complex realizations.

In summary, this paper examines the development of fingers in viscously unstable displacements in bimodal heterogeneous media by studying the concentration contours and the mixing zone length. The results are compared to media with periodic permeability with unimodal heterogeneity. The sequence of the flow regimes and their timings are compared for different wavelength combinations.

## Model Description

A 2D miscible displacement in the porous media is modeled based on mass conservation, Darcy's description of momentum conservation, and the convective-diffusive mass transfer between the miscible solutions. Fluid 1 is injected (from left) into the rectangular medium with uniform apparent velocity  $U$  and concentration  $\hat{C}_1$  to displace the resident fluid (fluid 2) of uniform concentration  $\hat{C}_2$ .

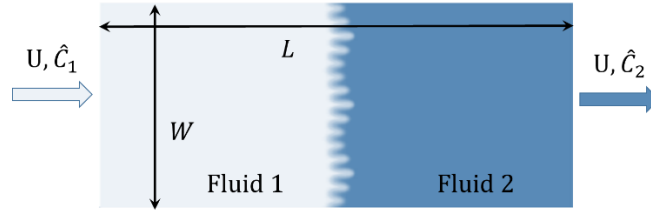


**Fig. 2.** Schematic of the modeled two-dimensional miscible displacement

The schematic of the model is shown in Fig.2, and the flow equations are as follows:

$$\hat{\nabla} \cdot \hat{\mathbf{u}} = 0 \quad (1)$$

$$\hat{\nabla} \hat{p} = -\frac{\hat{\mu} \hat{\mathbf{u}} \phi}{\hat{k}} \quad (2)$$

$$\frac{\partial \hat{C}}{\partial \hat{t}} + \hat{\mathbf{u}} \cdot \hat{\nabla} \hat{C} = D \hat{\nabla}^2 \hat{C} \quad (3)$$

In this model, the flow is assumed to be incompressible and Newtonian. In the governing equations given above, the hat sign refers to dimensional variables. So here  $\hat{\nabla}$  represents the gradient vector in dimensional space  $(\hat{x}, \hat{y})$ ,  $\hat{p}$  is the pressure,  $\hat{\mathbf{u}} = (\hat{u}_x, \hat{u}_y)$  is the interstitial velocity vector, and  $\hat{C}$  is the solvent concentration.  $\hat{\mu}(\hat{C})$ ,  $\phi$  and  $\hat{k}(\hat{x}, \hat{y})$  represent the fluid viscosity, and the medium's porosity and permeability respectively. The viscosity of the fluids is assumed to be solely a function of the solvent concentration, and the porosity of the medium is deemed constant. The permeability distribution is defined using an exponential function with two cosine terms with two wavelengths describing the permeability variations across the domain:

$$\hat{k}(\hat{x}, \hat{y}) = k_1 \exp \left[ \frac{1}{2} s \left( \cos \left( \frac{2\pi n_{y1} \hat{y}}{W} \right) + \cos \left( \frac{2\pi n_{y2} \hat{y}}{W} \right) \right) \right] \quad (4)$$

In the given definition  $s$  sets the range of variation of permeability.  $n_{y1}$ ,  $n_{y2}$ , are the two frequencies of the permeability variation along  $\hat{y}$  the axis and  $W$  represents width of the domain. Two sample permeability idealizations are illustrated in Fig. 3, one with a unimodal heterogeneity (a periodic distribution of 15 layers) and a bimodal medium with two heterogeneity wavelengths with  $n_{y1} = 15$  and  $n_{y2} = 3$ . In Fig. 3a the permeability profiles from a cross-sectional view are plotted for both media. In Fig. 3b and 3c, the permeability contours over the domain are shown.

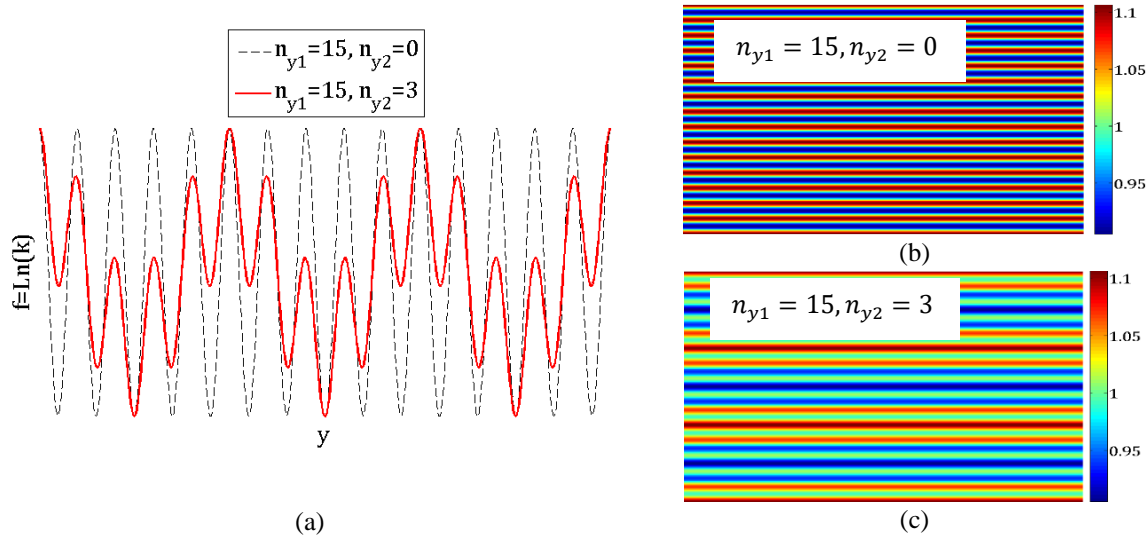


**Fig. 3.** Example of unimodal and bimodal heterogeneous field realizations, (a) permeability profiles on the cross-section of the porous medium, (b) permeability contour in the whole domain for a unimodal heterogeneous medium, (c) permeability contour in a bimodal heterogeneous medium

The viscosity-concentration correlation in this model is an exponential function [12].

$$\hat{\mu}(\hat{C}) = \hat{\mu}_1 \exp\left(R \left(\frac{\hat{C}_1 - \hat{C}}{\hat{C}_1 - \hat{C}_2}\right)\right) \quad (5)$$

This definition implies a viscosity of  $\hat{\mu}_1$  at the entrance, where the solvent concentration is  $\hat{C}_1$ , and a viscosity of  $\hat{\mu}_2 = \hat{\mu}_1 \exp(R)$  at the outlet with the solvent concentration of  $\hat{C}_2$ . Thus  $R$  represents the log viscosity ratio defined as  $\ln M = \ln \frac{\hat{\mu}_2}{\hat{\mu}_1}$ .

The equations are made dimensionless using diffusive scaling [7]. A Lagrangian reference frame attached to the displacement front is used. So the domain of interest moves with the flow, and the front remains at the center of the modeled frame at all times.

$$\begin{aligned} (x, y) &= \frac{(\hat{x} - U\hat{t}/\phi, \hat{y})}{D\phi/U} & t &= \frac{\hat{t}}{D\phi^2/U^2} & \mathbf{u} &= (u_x, u_y) = \frac{(\hat{u}_x, \hat{u}_y)}{U/\phi} \\ p &= \frac{\hat{p}}{D\hat{\mu}_1\phi/\hat{k}_1} & \mu &= \frac{\hat{\mu}}{\hat{\mu}_1} & k &= \frac{\hat{k}}{\hat{k}_1} & C &= \frac{\hat{C} - \hat{C}_2}{\hat{C}_1 - \hat{C}_2} \end{aligned} \quad (6)$$

The dimensionless equations can now be derived as:

$$\nabla \cdot \mathbf{u} = 0 \quad (7)$$

$$\nabla p = -\frac{\mu(\mathbf{u} + \mathbf{i})}{k} \quad (8)$$

$$\frac{\partial C}{\partial t} + \mathbf{u} \cdot \nabla C = \nabla^2 C \quad (9)$$

The permeability distribution and the viscosity-concentration function in dimensionless form can be written as follows:

$$k = \exp\left[\frac{1}{2} s \left( \cos\left(\frac{2\pi n_{y1} y}{WU/(D\phi)}\right) + \cos\left(\frac{2\pi n_{y2} y}{WU/(D\phi)}\right) \right)\right] \quad (10)$$

$$= \exp \left[ \frac{1}{2} s \left( \cos \left( \frac{2\pi n_{y1} y}{Pe/A} \right) + \cos \left( \frac{2\pi n_{y2} y}{Pe/A} \right) \right) \right]$$

$$\mu(C) = \exp(R(1 - C)) \quad (11)$$

where  $Pe = LU/(D\phi)$  is the Peclet number (also the dimensionless length of the domain) and  $A = L/W$  is the aspect ratio of the domain.

The details of the preparation of the equations for numerical simulation based on Hartley transformation are discussed in [13, 14] for non-isothermal displacements in homogeneous porous media and are briefly given in Appendix A for the heterogeneous system defined here. A semi-implicit second-order Adams-Bashforth-Adams-Moulton predictor-corrector is employed to solve Eq. A13. Other authors have previously used the numerical scheme and it has been validated against analytically predicted finger growth rates through linear stability analyses [15]. More details about the numerical technique is given in [14].

## Simulation Results

As stated in Eq. A6, the role of heterogeneity in the development of instability is defined by,  $\nabla f$  which is simplified to  $\frac{\pi s A n_y}{Pe} f$  for single frequency layered heterogeneity. Since  $f$  itself varies between -1 and 1 (regardless of the flow and medium's assigned parameters), the magnitude of  $\nabla f$  depends on the multiplied factor. Therefore, for given flow parameters in unimodal layered media, the influence of heterogeneity on the flow instability and mixing zone growth depends on the factor  $\frac{n_y}{Pe/A}$  (i.e. inverse of the dimensionless width of the layers), and the range of variation of permeability represented by  $s$ . For the scenarios discussed here, the range of permeability variations  $s$  and the dimensionless length of the medium  $Pe$  are kept constant. Thus the only difference between the permeability realizations is the length scale of heterogeneity. Although in this study, parameters of the same nature as the single frequency layered media are involved, the combination of two permeability profiles with different frequencies substantially alters the observed phenomena in the simple harmonic layered media. The reason is illustrated in Fig. 4, which shows how changing the number of layers varies  $\nabla f$  in single frequency and double frequency permeability profiles. For clarity, the curves are plotted over half of the width of the medium. As observed in these plots, the magnitude of the gradient of log permeability in unimodal heterogeneity is directly related to the number of layers. A 25-layer has a proportionally larger gradient than a 15-layer medium. But the same guideline does not apply to double permeability frequency profiles. The role of the second wavelength is noticed in comparing the two scenarios with  $n_{y1} = 15$ ,  $n_{y2} = 11$  and  $n_{y1} = 15$ ,  $n_{y2} = 3$ . The latter shows much a smaller magnitude of log permeability gradient. Also, a base wave of  $n_{y1} = 15$  layers combined with an 11 layer wave shows the same magnitude of  $\nabla f$  as the third case with  $n_{y1} = 25$ ,  $n_{y2} = 3$ .

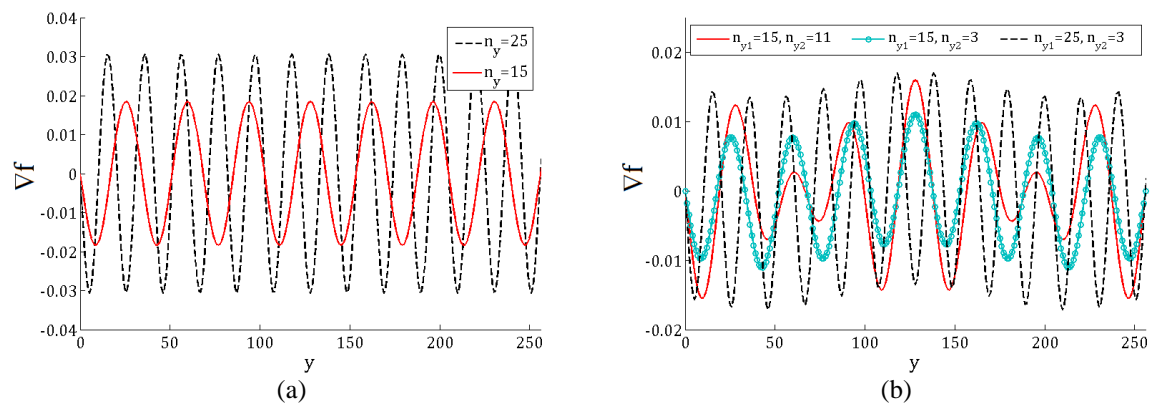


**Fig. 4.** Log permeability gradient  $\nabla f$  profiles for (a) unimodal heterogeneity, and (b) bimodal heterogeneity

In this part of the results section, the frequency of the base wave is kept constant as  $n_{y1} = 15$ , and the wavelength of the imposed wave is changed. In the next part, the effect of changing the base wave is investigated. In Fig.5, two reference scenarios are compared with the displacement in a bimodal medium. The reference cases belong to a 15 layer unimodal heterogeneous medium and a homogeneous porous medium. The third medium is defined by  $n_{y2} = 11$  on a base wave of  $n_{y1} = 15$ . The profile of the permeability across the flow direction is plotted on top of the first concentration contour for each scenario.

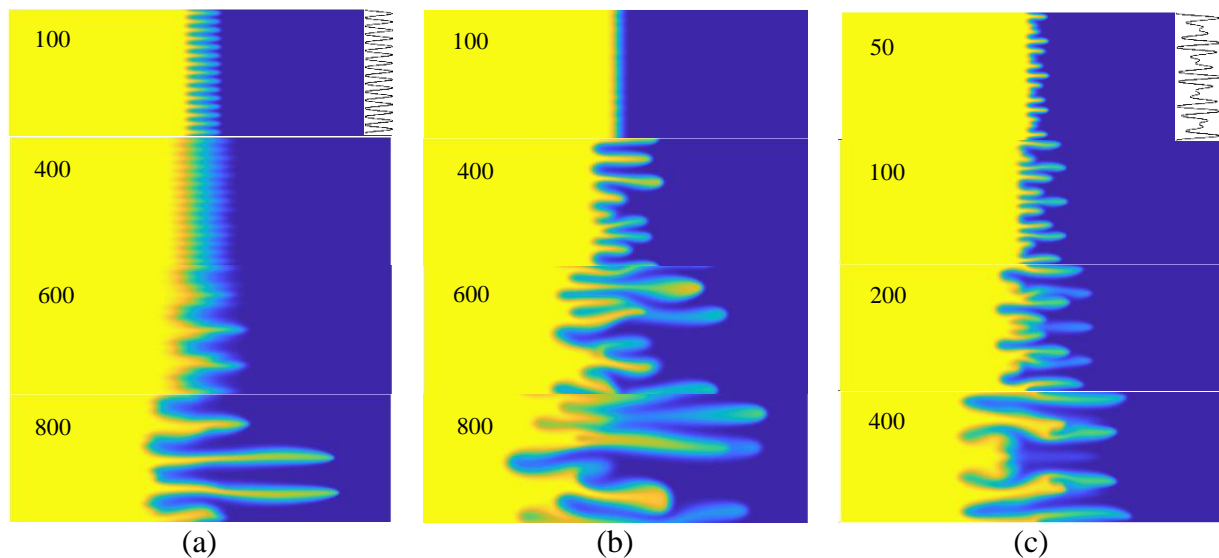


**Fig. 5.** Concentration contours of miscible displacements at different time steps in media with (a)  $n_y = 15$ , (b)  $n_y = 0$ , and (c)  $n_{y1} = 15, n_{y2} = 11$ . The setting parameters are  $Pe = 1024, A = 2, R = 3, s = 0.1$

In Fig.5a, in the 15 layer medium, the flow regimes including the initial growth of the fingers in the high permeable layers (at  $t = 100$ ), the lateral diffusion and merging of the fingers (at  $t = 400$ ), and finally the growth of viscous fingers on the diffused front (at  $t = 600$  and  $800$ ) are observed. In comparison, the front in the homogeneous medium of Fig.5b shows a random distribution of viscous fingers and delayed development of instability in the absence of heterogeneity as a driving force. It can also be observed that at different time steps, the severity of instability is different between the two reference scenarios, though the breakthrough time (considering the moving reference frame) is more or less similar for both. Addition of a second heterogeneity wavelength in Fig.5c ( $n_{y2} = 11$ ) has a significant influence on the pattern of fingers and their growth rate. Bearing in mind that the development of instability driven by the heterogeneity of the medium depends on the rate of spatial variation of permeability, it is expected that the base wave with smaller length scale acts faster in destabilization of the front than the second wave with a larger length scale. That is why in the early time frames of Fig.5c

(at  $t = 50$ ), fifteen fingers can be counted on the front. Although the initial stimulation of instability is driven by the base wave, similar to the unimodal case of Fig.5a, in the bimodal system of Fig.5c, the uneven development of the fingers impedes efficient transverse diffusion between them and allows for further enhancement of instability. Therefore the fingers reach the downstream boundary at a shorter time. In the absence of a lateral diffusion regime, the consecutive flow regimes observed in the 15 layers porous medium are not established in the bimodal case with a second heterogeneity wavelength.

Since the channeling regime lasts a shorter period in layers with smaller wavelengths, in Fig.5c with  $n_{y2} = 11$ , the flow regime is past the channeling regime and viscous fingering in the late time frames is observed. In Fig. 6, the frequency of the imposed wave is changed to  $n_{y2} = 1, 3, \text{ and } 7$ . In the cases shown in Fig. 6a to 6c, like in Fig.5c, the early time frames show fifteen fingers, which means that the base wave controls the instability at the early stages. By further progress of the displacement front, the growth of fingers in the wider channels becomes more apparent and the second wavelength takes over. Similar to Fig.5c, the combination of the wavelengths enhances the instability with respect to the simple 15-layer medium. Again the base wavelength helps faster stimulation of fingers and the imposed wavelength disturbs the transverse diffusion (hence skipping the diffusive flow regime) and guides the instability in a second mode of channeling.

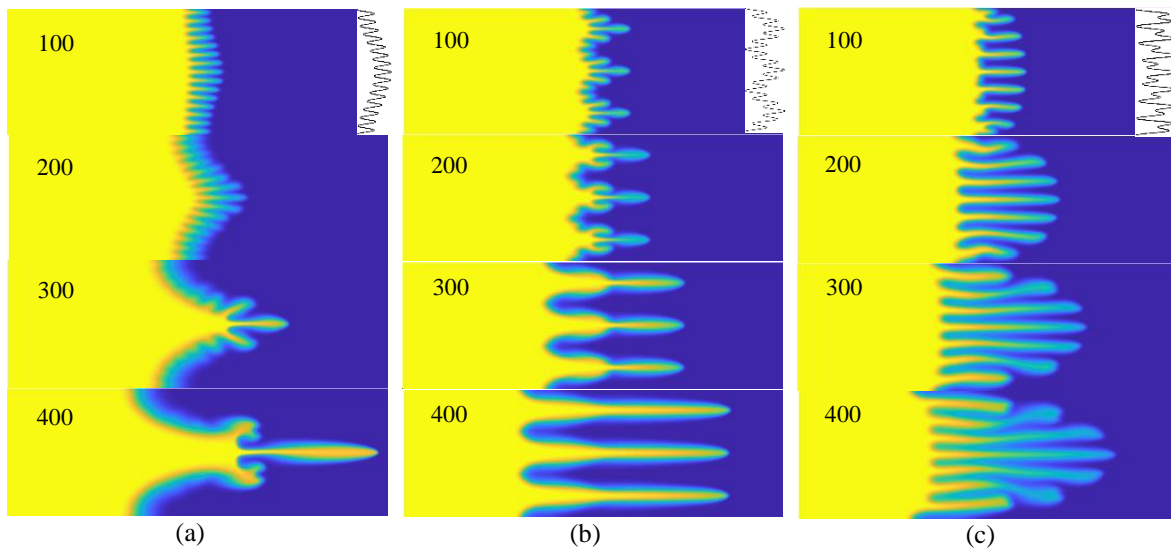


**Fig. 6.** Concentration contours of miscible displacements at different time steps in media with the base wave of  $n_{y1} = 15$ , the second wave of permeability variation imposed on the first wave has (a)  $n_{y2} = 1$ , (b)  $n_{y2} = 3$ , and (c)  $n_{y2} = 7$  layers. The setting parameters are  $Pe = 1024, A = 2, R = 3, s = 0.1$

For cases with  $n_{y2} = 1, 3, \text{ and } 5$  ( $n_{y2} = 5$  is not shown here due to its close similarity to the  $n_{y2} = 3$  scenario) since the second wave number is a factor of the base wave's number of layers, each wide finger absorbs a corresponding number of smaller fingers (15, 5, and 3 small fingers per a large finger, respectively), and the process of emerging is similarly repeated for each wide finger. Looking at Fig. 6b, for instance, the similarity between the three layers of the imposed wave suggests that the pattern can be repeated. So if the width of the medium,  $n_{y1}$  and  $n_{y2}$  are all doubled, then the fingering looks the same as in Fig. 6b. A similar concept has been reported by Rubin [10] for random bimodal heterogeneity, stating that the contribution of each mode depends on the ratio between the length scales. For  $n_{y2} = 7$  and 11 in Fig. 6c and Fig.5c, evolving of  $n_{y2}$  fingers from 15 fingers is uneven and although in the later times  $n_{y2}$  fingers are distinguished, they are not distributed as uniformly as the cases with  $n_{y2} = 1, 3$  and 5.

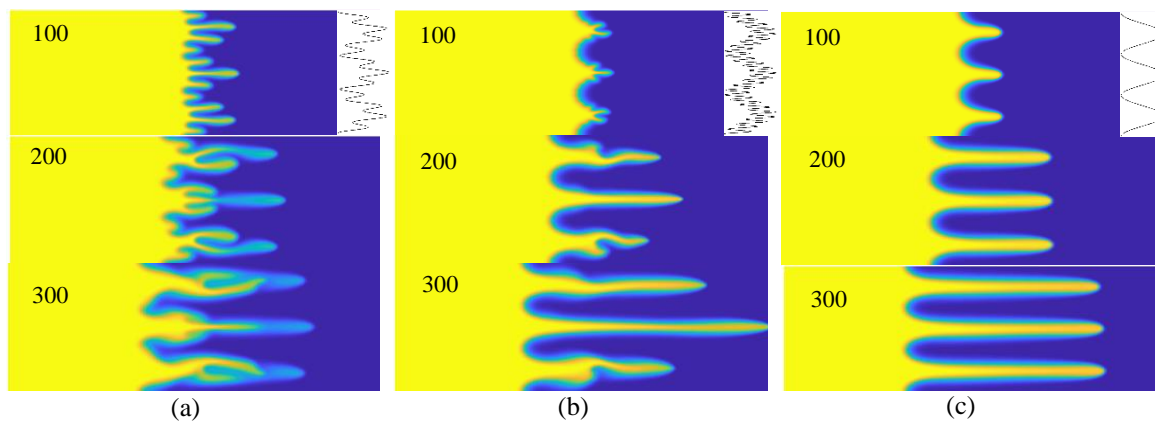


**Fig. 7.** Concentration contours of miscible displacements at different time steps in media with the second wave of permeability variation with  $n_{y2} = 3$  layers imposed on base wave of (a)  $n_{y1} = 11$ , (b)  $n_{y1} = 25$ , and (c)  $n_{y1} = 0$ . The setting parameters are  $Pe = 1024, A = 2, R = 3, s = 0.1$

In this part of the results section (shown in Fig. 7), the base wave is changed to  $n_{y1} = 11$  and 25 while the second wave number is kept constant at  $n_{y2} = 3$ . The displacement in a three-layer medium (with no base wave) is shown in Fig. 7c for reference. As mentioned earlier, the channeled fingers diminish faster into a diffused front in a medium with smaller heterogeneity wavelength. As a result, in Fig. 7b with  $n_{y1} = 25$ , at  $t = 100$  the fingers developed in the narrow channels of the base wave are smaller than in Fig. 7a with  $n_{y1} = 11$ . Comparing the rate of growth of fingers, it seems like the cases discussed here have more or less the same breakthrough time. So, we may conclude that the second wave number,  $n_{y2}$ , controls the breakthrough time of the displacements in bimodal heterogeneous media. In the analytical study of Rubin [10] the time dependent dominance of each wavelength in finger growth, has been reported and the effect of large-scale permeability variations became significant at large travel distances.

For a quantitative analysis of the influence of the defined heterogeneity on the formed instabilities, the temporal growth of MZL is plotted for the described scenarios. First, the plots corresponding to varied second wave numbers are discussed, and then the effect of the base wave will be analyzed. As shown in Fig. 8, the homogeneous medium (brought here for comparison with the heterogeneous scenarios) goes through a diffusive regime until  $t = 200$  and then viscous fingering supports fast growth of mixing zone length in the following time steps. The heterogeneous media, however, deviate from the diffusive flow regime at the early stages due to growing fingers inside the channels. Among the heterogeneous media, the medium with single frequency  $n_y = 15$  heterogeneity shows the slowest growth of MZL and the bimodal heterogeneity enhances the growth rate of instability compared to the single-mode heterogeneous medium with the frequency of the base wave. One can see in the magnified plot that even at the initial time steps the media with a second imposed wave of heterogeneity (except for  $n_{y2} = 1$ ) show more rapid growth of MZL than the unimodal medium. The lateral diffusion regime is hardly noticeable except for  $n_{y2} = 11$  for which a slight decay in growth rate can be observed at around  $t = 200$  which may be considered a short period of lateral diffusion.

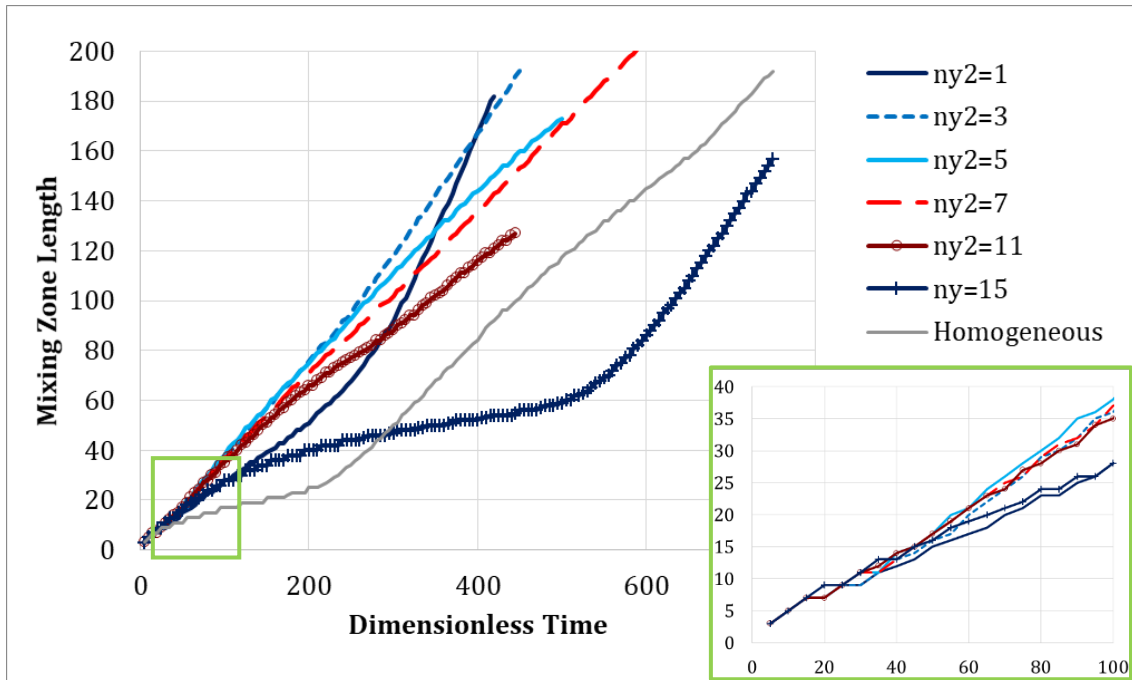


**Fig. 8.** Mixing zone length for media with two imposed permeability waves, the base wave for all the cases has 15 layers; the second imposed wave has smaller number of layers as show in the legend

The case with  $n_{y2} = 1$  follows the unimodal curve with  $n_y = 15$  for a longer period than the other scenarios. The reason lies in the fact that the longer wavelength corresponding to  $n_{y2} = 1$  acts more gradually in guiding the flow into the channel. So the effect of the second heterogeneity wavelength takes a longer time to appear on the MZL curve. The channeling regime lasts longer in wider channels, and the faster advancement of the instability in the final time frames of the process can be attributed to the channeling regime in the second heterogeneity wavelength. When the gap between the heterogeneity modes is large, they affect mixing in their separate time scale. A very small wavelength acts fast in destabilizing the front and then forming a diffused front which will later be directed into the larger wavelength channels. In the long period, it seems like a larger wavelength heterogeneity shows a faster growth of mixing zone and the MZL curves are ranged from large to small with respect to their assigned  $n_{y2}$  (with  $n_{y2} = 1$  showing the shortest breakthrough time and  $n_{y2} = 11$  the longest breakthrough time among the bimodal media). Similarly, in the numerical simulations of Amooie et al. [4] in media with a random distribution of low permeability facies, a faster breakthrough in media with scarce zones of higher permeability, which means larger length scale of heterogeneity, and more diffusive behavior in the zones with a smaller length scale of heterogeneity have been reported.

Fig. 9 shows the second set of results with constant wavelength heterogeneity ( $n_{y2} = 3$ ) imposed on different base waves. For reference, the displacements in a homogeneous porous medium and in a unimodal heterogeneous medium with  $n_y = 3$  are shown as well. Although the MZL curves show different breakthrough times, their slopes seem to be the same in the final stages of the flow as the fingers grow in  $n_{y2} = 3$  channels. If we look at the magnified graph, we can see more scattered curves compared to the early time curves of Fig.8. The reason is the dominance of the base wave in early time behavior which is different for the cases shown here in Fig. 9. In contrast to the previous cases, which showed enhanced instability for all bimodal distributions compared to the single wavelength scenario, when changing the base wave we

may see tempering of instability in bimodal cases. Yet overall, a smaller wavelength of the base wave seems to enhance instability at later times.

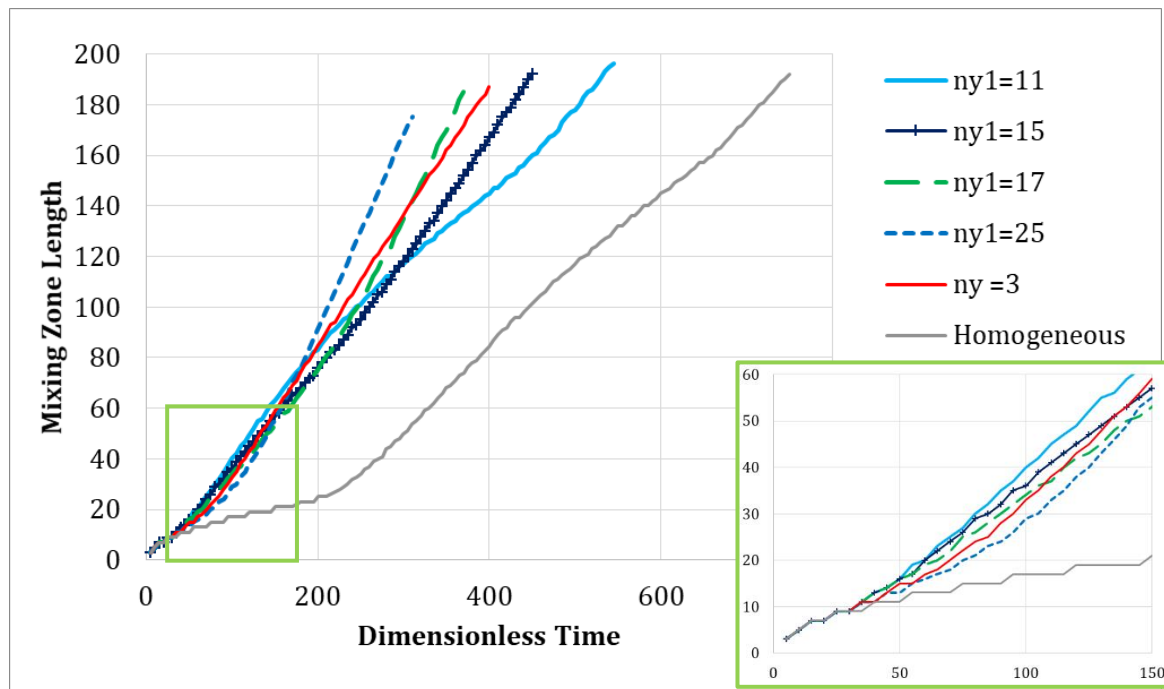


**Fig. 9.** Mixing zone length for media with two imposed permeability waves, the base wave for all the cases has 15 layers; the second imposed wave has smaller number of layers as show in the legend

## Conclusion

The interaction between viscous fingering and channeling in bimodal heterogeneous media has been investigated for miscible displacements through numerical simulation of the process. The heterogeneity has been defined as the combination of two cosine permeability profiles with different length scales to observe the effect of bimodal heterogeneity on the development of instabilities. Such a definition is aimed to provide a closer resemblance of reservoir rocks in a simple scheme in which the contribution of the involved parameters can be distinguished. Two sets of numerical experiments have been performed first, varying the imposed wave's wavelength of heterogeneity and keeping the base wave unchanged. In the second set a 3 layer periodic profile was imposed on different base waves. The concentration contours have been presented for qualitative examination of the emerging fingers on the displacement front. For quantitative analysis of the results, MZL profiles of the simulated cases have been compared.

The presence of a second wavelength in the permeability distribution profile changes the unstable flow regimes previously obtained for unimodal layered media. The instabilities at first follow the permeability distribution with the smaller wavelength (the base wave) but gradually merge into fingers formed in channels with larger wavelengths. The overlap of the flow regimes in double wavelength distributions enhances the instability compared to the unimodal medium with the base wave frequency. In the cases with large contrast between the wavelengths, the enhancement has been explained by the dominance of each mode at a different period. Faster growth of the mixing zone length in cases with close wave numbers between the combined waves (e.g., 15 layers combined with 11 layers) has been attributed to the fading of the lateral diffusion regime due to the dissimilar fingering patterns.

The base wave's frequency showed a non-uniform effect. The base waves with smaller wavelengths showed enhanced instability compared to the unimodal medium with the imposed wave's profile, while base waves with larger wavelengths attenuated the growth of fingers by delaying the dominance of the imposed wave.

## References

- [1] Abriola LM. Modeling contaminant transport in the subsurface: An interdisciplinary challenge. *Reviews of Geophysics*. 1987 Mar;25(2):125-34.
- [2] Broyles BS, Shalliker RA, Cherrak DE, Guiochon G. Visualization of viscous fingering in chromatographic columns. *Journal of Chromatography A*. 1998 Oct 2;822(2):173-87.
- [3] Fanchi JR. Principles of applied reservoir simulation. Elsevier; 2005 Dec 8.
- [4] Amooie MA, Soltanian MR, Xiong F, Dai Z, Moortgat J. Mixing and spreading of multiphase fluids in heterogeneous bimodal porous media. *Geomechanics and Geophysics for Geo-Energy and Geo-Resources*. 2017 Sep;3(3):225-44.
- [5] Enin A, Kalinin K, Petrova Y, Tikhomirov S. Optimal polymer slugs injection curves. arXiv preprint arXiv:2012.03114. 2020 Dec 5.
- [6] De Wit A, Homsy GM. Viscous fingering in periodically heterogeneous porous media. II. Numerical simulations. *The Journal of chemical physics*. 1997 Dec 8;107(22):9619-28.
- [7] Sajjadi M, Azaiez J. Scaling and unified characterization of flow instabilities in layered heterogeneous porous media. *Physical Review E*. 2013 Sep 23;88(3):033017.
- [8] Nijjer JS, Hewitt DR, Neufeld JA. Stable and unstable miscible displacements in layered porous media. *Journal of Fluid Mechanics*. 2019 Jun;869:468-99.
- [9] Cantrell DL, Hagerty RM. Microporosity in arab formation carbonates, Saudi Arabia. *GeoArabia*. 1999 Apr 1;4(2):129-54.
- [10] Rubin Y. Flow and transport in bimodal heterogeneous formations. *Water Resources Research*. 1995 Oct;31(10):2461-8.
- [11] Lu Z, Zhang D. On stochastic modeling of flow in multimodal heterogeneous formations. *Water Resources Research*. 2002 Oct;38(10):8-1.
- [12] Pritchard D. The instability of thermal and fluid fronts during radial injection in a porous medium. *Journal of Fluid Mechanics*. 2004 Jun;508:133-63.
- [13] Sajjadi M, Azaiez J. Dynamics of fluid flow and heat transfer in homogeneous porous media. *The Canadian Journal of Chemical Engineering*. 2013 Apr;91(4):687-97.
- [14] Islam MN, Azaiez J. Miscible thermo-viscous fingering instability in porous media. Part 2: Numerical simulations. *Transport in porous media*. 2010 Sep;84(3):845-61.
- [15] Meiburg E, Chen CY. High-accuracy implicit finite-difference simulations of homogeneous and heterogeneous miscible-porous-medium flows. *Spe Journal*. 2000 Jun 1;5(02):129-37.
- [16] Tan CT, Homsy GM. Simulation of nonlinear viscous fingering in miscible displacement. *The Physics of fluids*. 1988 Jun;31(6):1330-8.
- [17] Manickam O, Homsy GM. Fingering instabilities in vertical miscible displacement flows in porous media. *Journal of Fluid Mechanics*. 1995 Apr;288:75-102.
- [18] Bracewell R. *The Fourier Transform and Its Applications*. McGraw Hill, 2000 (34):712.
- [19] Bracewell R. Discrete Hartley transform. *Journal of Optical Society of America*, vol. 73, no. 12, pp. 1831-1835, 1983.
- [20] Shahnazari MR, Maleka Ashtiani I, Saberi A. Linear stability analysis and nonlinear simulation of the channeling effect on viscous fingering instability in miscible displacement. *Physics of Fluids*. 2018 Mar 27;30(3):034106.
- [21] Sheng JJ, editor. *Enhanced oil recovery field case studies*. Gulf Professional Publishing; 2013 Apr 10.

**How to cite:** Sajjadi M. The Influence of Bimodal Heterogeneity on Viscous Fingering of a Miscible Interface in Porous Media. Journal of Chemical and Petroleum Engineering. 2021; 55(1): 369-383.

## Appendix A

For solving the given set of dimensionless equations, the stream function-vorticity formulation of [14, 16] is adopted. First, the pressure is eliminated by taking the curl of Eq. 8, knowing that  $\nabla \times \nabla = 0$  for any continuously twice differentiable function. Thus:

$$\nabla \times \nabla p = -\nabla \times \left( \frac{\mu(\mathbf{u} + \mathbf{i})}{k} \right) \quad (\text{A } 1)$$

$$\frac{k}{\mu} \nabla \left( \frac{\mu}{k} \right) \times (\mathbf{u} + \mathbf{i}) = -\nabla \times (\mathbf{u} + \mathbf{i})$$

One can apply the operator to obtain  $\nabla \times (\mathbf{u} + \mathbf{i}) = \nabla \times \mathbf{u}$ , which is the definition of vorticity vector  $\boldsymbol{\omega}$ . Also  $\frac{k}{\mu} \nabla \left( \frac{\mu}{k} \right) = \nabla \left( \ln \frac{\mu}{k} \right)$  hence Eq. (A 1) reduces to:

$$\begin{aligned} \boldsymbol{\omega} &= -\nabla \left( \ln \frac{\mu}{k} \right) \times (\mathbf{u} + \mathbf{i}) \\ &= -\nabla(\ln \mu) \times (\mathbf{u} + \mathbf{i}) + \nabla(\ln k) \times (\mathbf{u} + \mathbf{i}) \end{aligned} \quad (\text{A } 2)$$

Incorporating Eq. 10 and Eq. 11 we have:

$$\nabla(\ln \mu) = -R\nabla C \quad (\text{A } 3)$$

$$\nabla(\ln k) = -\frac{\pi s}{\text{Pe}} \left\{ A \left( n_{y1} \sin \left( \frac{2\pi n_{y1} y}{\text{Pe}/A} \right) + n_{y2} \sin \left( \frac{2\pi n_{y2} y}{\text{Pe}/A} \right) \right) \right\} \quad (\text{A } 4)$$

For brevity, we keep  $\nabla(\ln k) = \nabla f$  thus Eq. A2 can be expanded to:

$$\begin{aligned} \boldsymbol{\omega} &= R\nabla C \times (\mathbf{u} + \mathbf{i}) + \nabla f \times (\mathbf{u} + \mathbf{i}) \\ \boldsymbol{\omega} &= -R \left( \frac{\partial C}{\partial x} u_y - \frac{\partial C}{\partial y} (u_x + 1) \right) - \left( \frac{\partial f}{\partial x} u_y - \frac{\partial f}{\partial y} (u_x + 1) \right) \end{aligned} \quad (\text{A } 5)$$

Where  $\frac{\partial f}{\partial x}$  and  $\frac{\partial f}{\partial y}$  are the components of the vector defined in Eq. A4. In fluid mechanics the stream function is defined as a scalar integral whose derivative gives the velocity vector as  $\frac{\partial \psi}{\partial y} = u_x$  and  $\frac{\partial \psi}{\partial x} = -u_y$  which can be adopted in Eq. A5 to give:

$$\begin{aligned} \boldsymbol{\omega} &= R \left( \frac{\partial C}{\partial x} \frac{\partial \psi}{\partial x} + \frac{\partial C}{\partial y} \left( \frac{\partial \psi}{\partial y} + 1 \right) \right) + \left( \frac{\partial f}{\partial x} \frac{\partial \psi}{\partial x} + \frac{\partial f}{\partial y} \left( \frac{\partial \psi}{\partial y} + 1 \right) \right) \\ &= (R\nabla C + \nabla f) \cdot (\nabla \psi + \mathbf{j}) \end{aligned} \quad (\text{A } 6)$$

For an incompressible flow by definition  $\boldsymbol{\omega} = -\nabla^2 \psi$ . Hence the system of equations to be solved *now* consists of:

$$\begin{aligned}
 \omega &= (R\nabla C + \nabla f) \cdot (\nabla\psi + \mathbf{j}) \\
 \omega &= -\nabla^2\psi \\
 \frac{\partial C}{\partial t} + \mathbf{u} \cdot \nabla C &= \nabla^2 C
 \end{aligned} \tag{A 7}$$

The boundary and the initial conditions can be defined based on the described model as:

$$\begin{aligned}
 (\omega, C)(x, y, t_0) &= (0, C_0) \\
 (\omega, C)(0, y, t) &= (0, 1) \\
 (\omega, C)(Pe, y, t) &= (0, 0) \\
 (\omega, C)(x, 0, t) &= (\omega, C)(x, Pe/A, t)
 \end{aligned} \tag{A 8}$$

where  $C_0 = \frac{1}{2} \operatorname{erfc} \frac{x}{2\sqrt{t_0}}$ . The numerical method is based on the transformation of the equations to Hartley space. Application of this pseudo-spectral method requires periodic boundary conditions. Hence, the concentration is decomposed to the base state and perturbed concentration  $C = \bar{C} + C'$  as suggested by [17]. The base state is obtained from solving the unperturbed convection-diffusion equation with the uniform injection velocity throughout the domain defined by  $\frac{\partial \bar{C}}{\partial t} = \nabla^2 \bar{C}$ . For the defined boundary and initial conditions:

$$\bar{C} = \frac{1}{2} \operatorname{erfc} \frac{x}{2\sqrt{t}} \tag{A 9}$$

Thus the system of equations is now expressed (and solved) in terms of the new unknown perturbed concentration  $C'$ .

$$\begin{aligned}
 \omega &= \left( R\nabla C' + R \frac{\partial \bar{C}}{\partial x} \mathbf{i} + \nabla f \right) \cdot (\nabla\psi + \mathbf{j}) \\
 \omega &= -\nabla^2\psi \\
 \frac{\partial C'}{\partial t} + \mathbf{u} \cdot \nabla C' + \mathbf{u} \cdot \nabla \bar{C} &= \nabla^2 C'
 \end{aligned} \tag{A 10}$$

With the periodic boundary conditions defined for  $C'$

$$\begin{aligned}
 (\omega, C')(x, y, t_0) &= (0, 0) \\
 (\omega, C')(0, y, t) &= (0, 0) \\
 (\omega, C')(Pe, y, t) &= (0, 0) \\
 (\omega, C')(x, 0, t) &= (\omega, C')(x, Pe/A, t)
 \end{aligned} \tag{A 11}$$

The deviation in concentration field from the base-state profile can be triggered by the initial perturbation, which later grows into viscous fingers or permeability variations. In the absence of these causes, the flow remains stable, and the concentration follows  $\bar{C}$  profile. It should be emphasized that the definition of  $\bar{C}$  is optional, and any step-like function that is twice differentiable can maintain the periodic boundary condition for the remaining  $C'$ . In fact, the periodic boundary condition required for application of Hartley based (or any other) spectral method may be achieved by doubling the length of the domain and mirroring the concentration profile as done by Tan and Homsy [16]. But this scheme doubles the size of the simulated domain and consequently the computational complexity. Tan and Homsy used the Fourier transformation for solving the exact system of equations for homogeneous porous media. Hartley transform is closely related to Fourier transform with the advantage of retaining the transformed functions in the real space and is equally applicable for inverse transformation.

In this work a two-dimensional Fast Hartley Transformation (FHT) has been employed for the enhancement of accuracy of the numerical simulations [18]. The method has been successfully applied to simulate viscous fingering [7, 13, 14, 17]. The discrete Hartley transform of function  $g(x, y, t)$ , and its partial derivatives, are defined as [19]:

$$\begin{aligned}
 H[g(x, y, t)](q_x, q_y) &= \frac{1}{\sqrt{N_x N_y}} \sum_{i=1}^{N_x} \sum_{j=1}^{N_y} g(x_i, y_j, t) (\cos(q_y y_j) + \sin(q_y y_j)) (\cos(q_x x_i) + \sin(q_x x_i)) \\
 H\left[\frac{\partial g}{\partial x}(x, y, t)\right](q_x, q_y) &= -2\pi q_x H[g(x, y, t)](-q_x, q_y) H\left[\frac{\partial^2 g}{\partial x^2}(x, y, t)\right](q_x, q_y) \\
 &= -4\pi^2 q_x^2 H[g(x, y, t)](q_x, q_y)
 \end{aligned} \tag{A 12}$$

To avoid redundancy, only the transformation of partial derivatives concerning one variable are presented. Here  $N_x$  and  $N_y$  are the number of spectral modes or the number of grids along  $x$  and  $y$  axes.  $q_x$  and  $q_y$  are the variables of the spectral domain, and  $x_i = 2\pi i/N_x$  and  $y_j = 2\pi j/N_y$ . The Hartley transform of a function is going to be shown with a tilde sign. Thus the system of equations and the corresponding initial condition defined in A10 and A11 will be transformed into A13 and A14, respectively:

$$\begin{aligned}
 \tilde{\omega} &= H\left[\left(R\nabla C' + R\frac{\partial \tilde{C}}{\partial x}\mathbf{i} + \nabla f\right) \cdot (\nabla\psi)\right] - 2\pi R q_y \tilde{C}'(q_x, -q_y) \\
 &\quad - 2\pi R q_y \tilde{f}(q_x, -q_y) \\
 \tilde{\omega} &= 4\pi^2 (q_x^2 + q_y^2) \tilde{\psi}
 \end{aligned} \tag{A 13}$$

$$\begin{aligned}
 \frac{\partial \tilde{C}'}{\partial t} + H[\mathbf{u} \cdot \nabla C' + \mathbf{u} \cdot \nabla \tilde{C}] &= -4\pi^2 (q_x^2 + q_y^2) \tilde{C}' \\
 (\tilde{\omega}, \tilde{C}') &(q_x, q_y, t_0) = (0, 0)
 \end{aligned} \tag{A 14}$$

Note that the boundary conditions are no longer required in the spectral domain as the spatial derivatives are transformed. The nonlinear terms need to be calculated in the real domain and then transformed to Hartley space.